Adjacent Axial Ligand Enables Secondary Coordination Effects in Metal-Nitrogen-Carbon Towards Improved Scaling Relation of Oxygen Electrocatalysis

Ke Ye[a,b†], Yulan Han[c†], Min Hu[a]*, P. Hu[c,d], Mårten S. G. Ahlquist[b]*, Guozhen Zhang[a,e]*

[a] Hefei National Research Center for Physical Sciences at the Microscale, School of Chemistry and Materials Science, University of Science and Technology of China, Hefei, Anhui 230026, China.
[b] Department of Theoretical Chemistry and Biology, KTH Royal Institute of Technology, 10691 Stockholm, Sweden
[c] School of Chemistry and Chemical Engineering, Queen's University Belfast, Belfast BT9 5AG, U.K.
[d] School of Physical Science and Technology, ShanghaiTech University, Shanghai 201210, China.
[e] School of Future Technology, University of Science and Technology of China, Hefei, Anhui 230026, China.

Abstract

Heterogenous single-atom catalysts (SACs) are reminescent of homogenous catalysts because of similarity of structural motif of active sites, opening a window for applying merits of homogenous catalysts to address issues in hetereogenous catalysis. In heterogeneous oxygen electrocatalysis, the homogeneity of adsorption patterns of reaction intermediates leads to scaling relationships that limit their activities. In contrast, homogeneous catalysts can circumvent such limits by selectively altering the adsorption of intermediates through secondary coordination effects (SCE). This inspired us to explored SCE in metal-nitrogen-carbon (M-N-C), a promising type of oxygen electrocatalysts. First-principles calculations on M-N-C containing two adjacent four-nitrogen-coordinated metal centers show that axial ligand in proximate active sites induces SCE that selectively stabilize OOH intermediate, disrupt scaling relation between oxygen-species, and eventually increase the catalytic activity in oxygen evolution reactions. Additionally, the activity of oxygen reduction reaction of selected M-N-C is also enhanced by such SCE. Our computational work underscored

the critical role of SCE in shaping activities of SACs, particularly in breaking stubborn scaling relationships, and demonstrated its potential of leveraging it to tackling challenges in heterogeneous catalysis.

Introduction

The emergence of single-atom catalysis (SACs)[1] not only paves a path for creating a new type of heterogeneous catalysts that combines high activity and economic utilization of transition metal atoms but also provides a promising architecture of catalyst that can fuse advantages of conventional heterogeneous and homogeneous catalysts[2-6]. In the past decade, with the aid of sophisticated experimental techniques and computational tools, scientists have made substantial progress in both crafting well-controlled structures and understanding the working mechanisms of SACs[7-13]. It is well-accepted that the local environment around metal centers in SACs plays a crucial part in shaping their electronic structures and ensuing catalytic activity and selectivity[3, 9, 12], including the coordinating atoms of metal centers[7, 14], the multi-adsorption effects[15-17], and the strength of metal-support interaction[18]. Intriguingly, most of these studies have primarily focused on the first coordination layer[4, 8, 10-12, 19], with less attention paid to the secondary[20] and even more distant coordination shells of metal centers in SACs. Meanwhile, in enzymatic and homogeneous catalysis, the secondary coordination shell is known to play an important role in determining the performance of the catalyst of interest[21-29]. Besides, with the advent of increasing amounts of high-density SACs, the impact of secondary coordination becomes inevitable[30-31]. Even though SACs are praised for combining the features of heterogeneous and homogeneous catalysis, investigations of the secondary coordination effects on SACs are scarce.

For heterogeneous catalysis, the scaling relationship between the adsorption energies of intermediates limits the performance of the catalysts, including nitrogen reduction reaction (NRR), CO_2 reduction reaction (CO_2RR), oxygen evolution reaction (OER), and oxygen reduction reaction (ORR)[13, 28, 31-35]. Taking OER and ORR on

transition metal surfaces as examples, the universal scaling relationship between the adsorption energies of key intermediates(*OH, *O, and *OOH), represented by $\Delta G_{*O} = 2\Delta G_{*OH}$ and $\Delta G_{*OOH} = \Delta G_{*OH} + 3.2$, set a theoretical limit of the overpotential at 370 mV for the most active metal[36]. Highly active single-sites in SACs cannot be free from these scaling relations as well[30-31, 37]. It mainly originates from the homogeneity of the adsorption of intermediates, meaning that the adsorption site and pattern of different intermediates are not changed during the reaction process[38]. Meanwhile, enzymes and molecular catalysts can break the homogeneity of adsorption and bypass the limit with the help of the secondary coordination ligands, which selectively tune the adsorption of intermediates or changing the mechanism from water nucleophilic attack(WNA) to (interaction of two metal-oxo entities) I2M[28, 39-40]. Craig et al. found that the intramolecular H-bonding between *OOH and ligands can be leveraged to improve the scaling[28]. Matheu et al. showed that H-bonding between dangling carboxylate group and *OOH can be leveraged to boost the kinetics of the *O to *OOH step in the WNA mechanism[41]. Theoretical investigations have also predicted that the second coordination sphere could modulate the binding energy of the crucial *O intermediate[42]. For high-density SACs, the proximity of two discrete active centers has been used as a knob to alter scaling relations in heterogeneous catalysis[30-31], hinting the possibility of similar secondary coordination effects (SCE) in such model systems.

To test our hypothesis on SCE in high-density SACs, we chose OER and ORR as the reactions of interest because of their well-estabilished scaling relations. We used the metal-nitrogen-carbon (M-N-C) materials in which MN_4 fragments are anchored in the plane of defected graphene as model SACs because of the ease of synthesis[43-44] and their potential of being cost-effective OER and ORR catalysts[45-46]. Through periodic spin-polarized density-functional theory calculations, we found that SCE can disrupt the scaling relationships of OER and ORR in two ways: (1) SCE disrupt the scaling relation between ΔG_{*O} and ΔG_{*OH} ($\Delta G_{*O} = 2\Delta G_{*OH}$ on the pure metal surface[32, 36]); (2) SCE selectively stabilizes *OOH without strengthening the adsorption of *OH,

which decreases the free energy change from *OH to *OOH ($\Delta G_{*OOH} = \Delta G_{*OH} + 3.2$ eV on the pure metal surface [32, 36], and the ideal intercept is 2.46 eV). As a result, we obtained more favorable energetics of OER and ORR with the help of SCE, which convert into better turnover-frequencies, as supported by a kinetics model. Our study demonstrates the significance of exploring the secondary coordination effects in heterogeneous SACs and leveraging them for enhanced catalytic performances.

Results and discussion

We first built 28 M-N-C models (denoted as MN_4/G) differing by the element type of metal center (Fig. 1a), some of which have been reported in both experimental and theoretical studies[4, 47]. Then the thermodynamic and electrochemical stabilities of these MN_4/G structures were assessed by formation energy and dissolution potential[30, 48]. Those in the upper left zone of Fig. 1b (negative formation energy and positive dissolution potential) are energetically more favorable, covering many experimentally synthesized MN_4/G SACs (M=Fe, Ni, Cu, Zn, Ru, Rh, Pd, and Ir)[44]. For OER and ORR intermediates (*OH, *O, and *OOH) adsorbed on these catalysts, as shown in Figs. 1c and 1d, their adsorption free energies exhibit strong scaling relationships, i.e. $\Delta G_{*O} = 1.82\Delta G_{*OH} + 1.01$, $\Delta G_{*OOH} = 0.75\Delta G_{*OH} + 3.2$. For the scaling between ΔG_{*OH} and ΔG_{*OOH}, as shown in Fig. 1e, albeit MN_4/G(black line) have improved scaling than pure metal surfaces(red line)[36], they are still distant from the volcano's summit (center of red triangle). The main reason lies in the large intercept value (3.2 eV) in the scaling equation ($\Delta G_{*OOH} = 0.75\Delta G_{*OH} + 3.2$), which results in a more positive ΔG_{*OOH}, indicating a weaker binding of *OOH. To mitigate this disadvantage, we have tried incremental tuning the first coordination shell of MN_4 site by replacing N atoms with C atoms. The resulting MN_3C/G, MN_2C_2/G, and MC_4/G still obey appreciable scaling relationships (Figs. 1f and 1g) in the adsorption energies of these three intermediates. Especially for *OOH and *OH (Fig. 1g), the minor change is too trivial to alter the corresponding catalytic activities in OER. There would be no significant difference in scaling relationships in adsorption energies than adsorption free energies because the

gap between these two energy terms is contributed by zero-point energy and entropy item of adsorbates, which we expect are comparable before and after the adsorption. The failure of altering scaling relations by modulating first coordination shell prompted us to examine the secondary coordination shell.

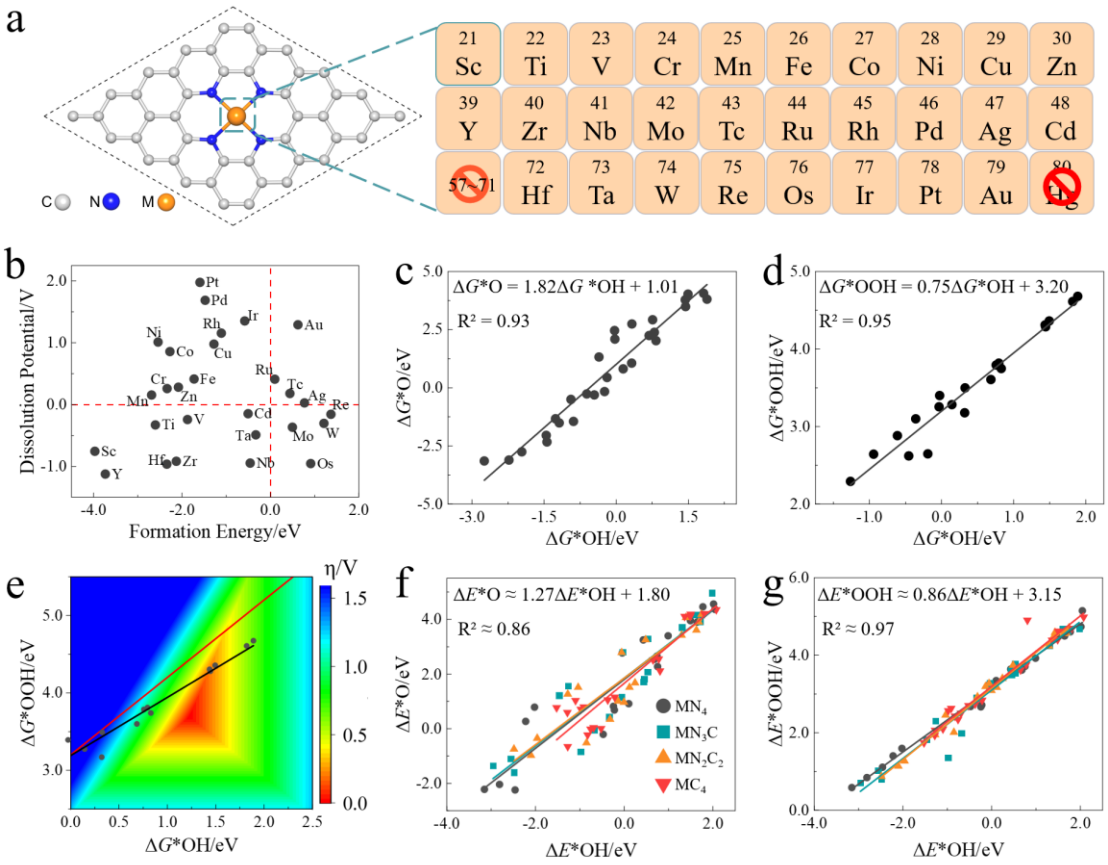

Figure 1. a) The structural prototype of MN_4/G. b) formation energy and dissolution potential of MN_4/G. c) the scaling relationships between ΔG_{*O} and ΔG_{*OH}. d) the scaling relationships between ΔG_{*OOH} and ΔG_{*OH}. e) 2-D volcano plot for OER, the red line represents the scaling relationship between *OOH and *OH on metals($\Delta G_{*OOH}=\Delta G_{*OH}+3.2$), and the black line represents the scaling relationship between *OOH and *OH on MN_4/G. f) the scaling relationships between ΔE_{*O} and ΔE_{*OH} on MN_xC_{4-x}/G(x=0, 2, 3, 4). g) the scaling relationships between ΔE_{*OOH} and ΔE_{*OH} on MN_xC_{4-x}/G(x=0, 2, 3, 4).

To construct a model that incorporates the outer coordination shell of single metal center, we first tested a dual active-center model, i.e. ho-2-MN_4/G, which have been demonstrated to disrupt linear relationships in NRR[30, 49]. As shown in Fig. 2a, a total of 28 kinds of ho-2-MN_4/G can be divided into three groups based on how *OOH is

relaxed on metal center(s): (1) indigo group (strong adsorption): *OOH directly decomposes into *O and *OH, each of them is one of two metals; (2) orange group (medium adsorption): *OOH is on one metal center and the other is idle; (3) brick red group (weak adsorption): *OOH bridges with two metal centers. Then adsorption energies of groups 2 and 3 were used to plot the scaling relation between ΔE_{*OOH} and ΔE_{*OH} (Figs. 2b). Little change has been found compared to the counterpart in mono MN_4/G (Fig. 1g), indicating the ho-2-MN_4/G model hardly improved the OER activity. Usually, breaking the scaling relationship requires both two active sites involved during the reaction[30, 35, 49]. Here, although a second MN_4 site is introduced, this MN_4 site does not participate in the reaction. So we speculate that it might be due to the large distance between the two metal centers. Then we tried a model with a shorter metal-metal distance (Fig. 2c), but still failed to substantially alter the scaling relationship between *OH, and *OOH (Fig. 2c). In addition, we examined other duo MN_4/G models with different two-dimensional carbon support environments, including MN_4/G within bilayer graphene of different interlayer distances and carbon nanotube of different diameters, but obtained similar scaling relationships between ΔE_{*OOH} and ΔE_{*OH} (Fig. S1, S2, and S3). Simply introducing a second adjacent metal center just did not bring SCE that can change existing scaling relationships in OER.

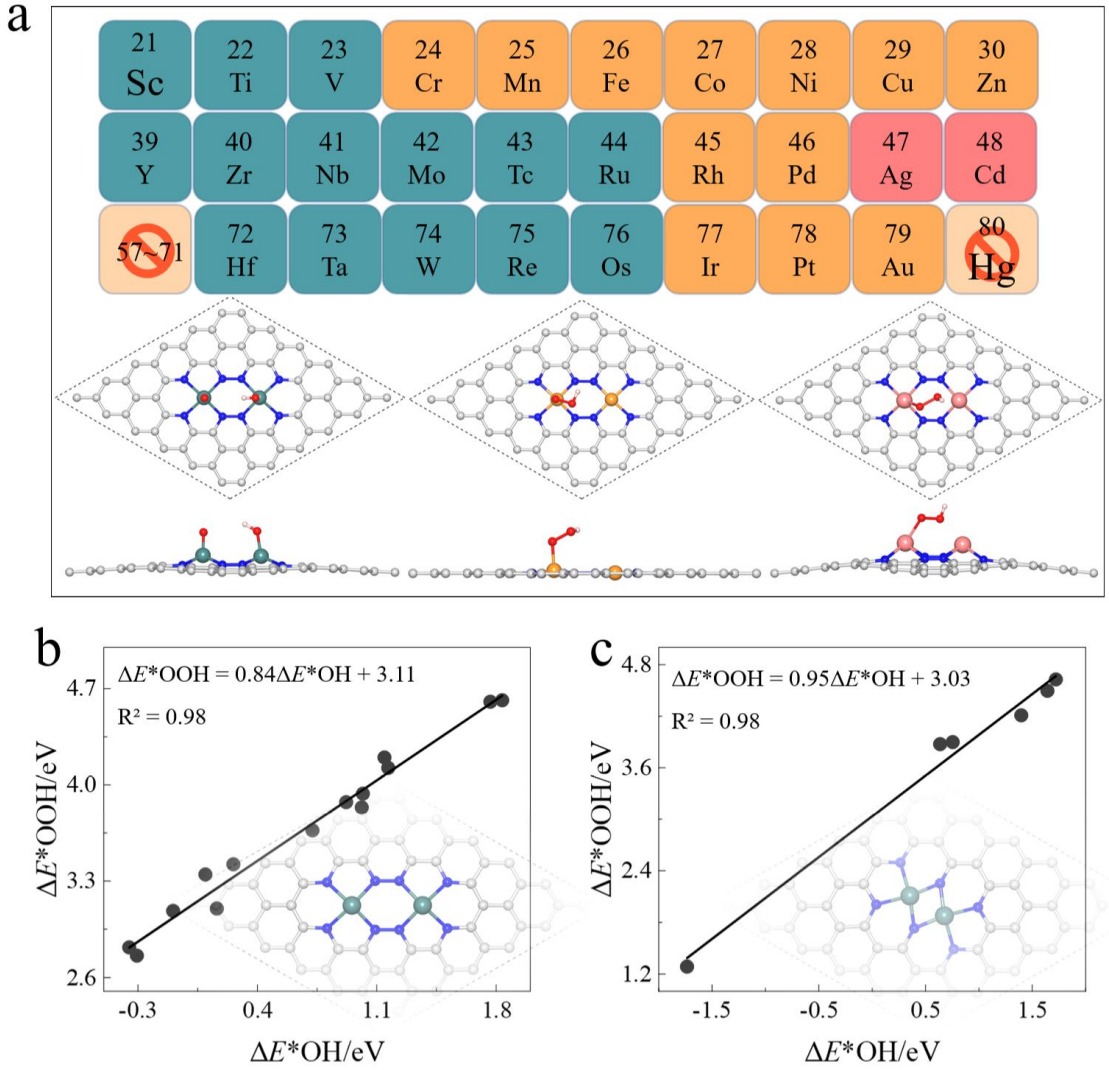

Figure 2. a) Three kinds of *OOH adsorption manners on ho-2-MN_4/G. b) the scaling relationships between on ΔE_{*OH} and ΔE_{*OOH} on ho-2-MN_4/G. c) the scaling relationships between ΔE_{*OH} and ΔE_{*OOH} on homonuclear duo MN_4/G model with two MN4 sites getting closer compared to ho-2-MN_4/G.

As shown in Fig. 3a, the adsorption of OH on selected metal centers (inside indigo oval) is much stronger, which makes it thermodynamically unfavorable to be converted into *O of OER because of large ordinate value (ΔE_{*O}-ΔE_{*OH}). Consequently, OH may stay on these oxygen-philic metal centers, making them potential secondary coordination ligands for the adjacent metal center, similar to the secondary coordination ligands in homogeneous catalysis[28]. Then we selected 4 types of $M1N_4$ (M1= Cd, Sc, Y, and Zn) to host OH based on the relative strength of OH adsorption on each $M1N_4$, and 6 types of $M2N_4$ (M2=Ag, Co, Cu, Ir, Ni, and Rh) as potential active centers for OER. A total of 24 combinations of $M1N_4$-$M2N_4$/G were generated and the

corresponding adsorption energies of *OH, *O, and *OOH were calculated using the same procedure. In the presence of *OH on M1 sites (denoted as *OH(M1)), the linear scaling of adsorption free energies on M2 sites between *O and *OH (Fig. 3b) is substantially weakened (R^2 decreased from 0.93 in MN_4/G to 0.54 in $M1N_4$-$M2N_4$/G) and that between *OH and *OOH (Fig. 3c) shifts down and gets a smaller intercept (getting closer to ideal intercept 2.46). As a result, the new scaling is closer to the theoretical peak in the contour map (Fig. 3d), suggesting a chance of finding a more active OER catalyst than MN_4/G.

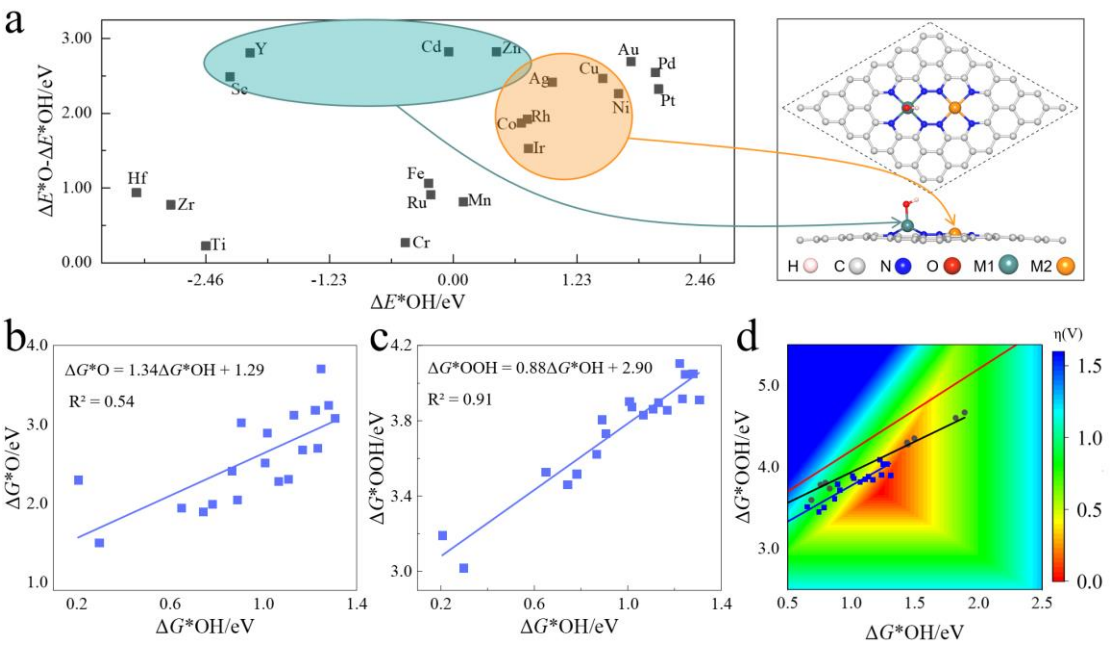

Figure 3. a) The distribution of MN_4/G along the ΔE_{*OH} and ΔE_{*O} - ΔE_{*OH}. And the structural prototype of $M1N_4$-$M2N_4$/G at the right side. b) the scaling relationship between ΔG_{*OH} and ΔG_{*O} on $M1N_4$-$M2N_4$/G. c) the scaling relationship between ΔG_{*OH} and ΔG_{*OOH} on $M1N_4$-$M2N_4$/G. d) 2-D volcano plot for OER, the red line represents the scaling relationship for ΔG_{*OOH} and ΔG_{*OH} on metals, the black line represents the scaling relationship for ΔG_{*OOH} and ΔG_{*OH} on MN_4/G, and the blue line represents the scaling relationship for ΔG_{*OOH} and ΔG_{*OH} on $M1N_4$-$M2N_4$/G.

Following the improvement of the scaling relationship between *OH and *OOH from MN_4/G to $M1N_4$-$M2N_4$/G, we conducted a more comprehensive kinetics analysis based on energetic data of every step in OER process, to examine that if SCE enhanced $M1N_4$-$M2N_4$/G by *OH(M1) is potentially a better OER catalyst than MN_4/G. The details of kinetics calculations using the CatMAP software package[50] have been

recorded in the SI. As shown in Fig. 4a and 4b, the contour map of $M1N_4$-$M2N_4$/G (Fig. 4b) not only has more data points closer to the peak than MN_4/G (Fig. 4a) but also possesses a substantially larger area with noticeable OER activity. Therefore, we have a larger likelihood of locating an efficient OER catalyst within $M1N_4$-$M2N_4$/G than MN_4/G, supporting our hypothesis about the promotive SCE role of *OH(M1) on OER.

To further validate whether SCE can effectively enhance OER catalytic performance occurring on $M1N_4$-$M2N_4$/G, we calculated the free energy diagrams covering the full set of elementary steps on six of the selected model systems (Fig. 4). Compared each MN_4/G, the counterpart $M1N_4$-$M2N_4$/G enjoys varying degrees of decrease of overpotential with the aid of *OH(M1). Among these $M1N_4$-$M2N_4$/G systems, *OH(Sc) gives NiN_4/G the largest improvement (a decrease by 0.57 V) in overpotential, and *OH(Zn) gives IrN_4/G the lowest overpotential of 0.24 V. For the reverse reaction of OER, i.e. ORR, the SCE of *OH(M1) will also enhance the ORR activity, as illustrated in Fig S6. The best combination is ScN_4-RhN_4/G with an overpotential of 0.22 V in ORR, in which the secondary ligand OH binds to Sc.

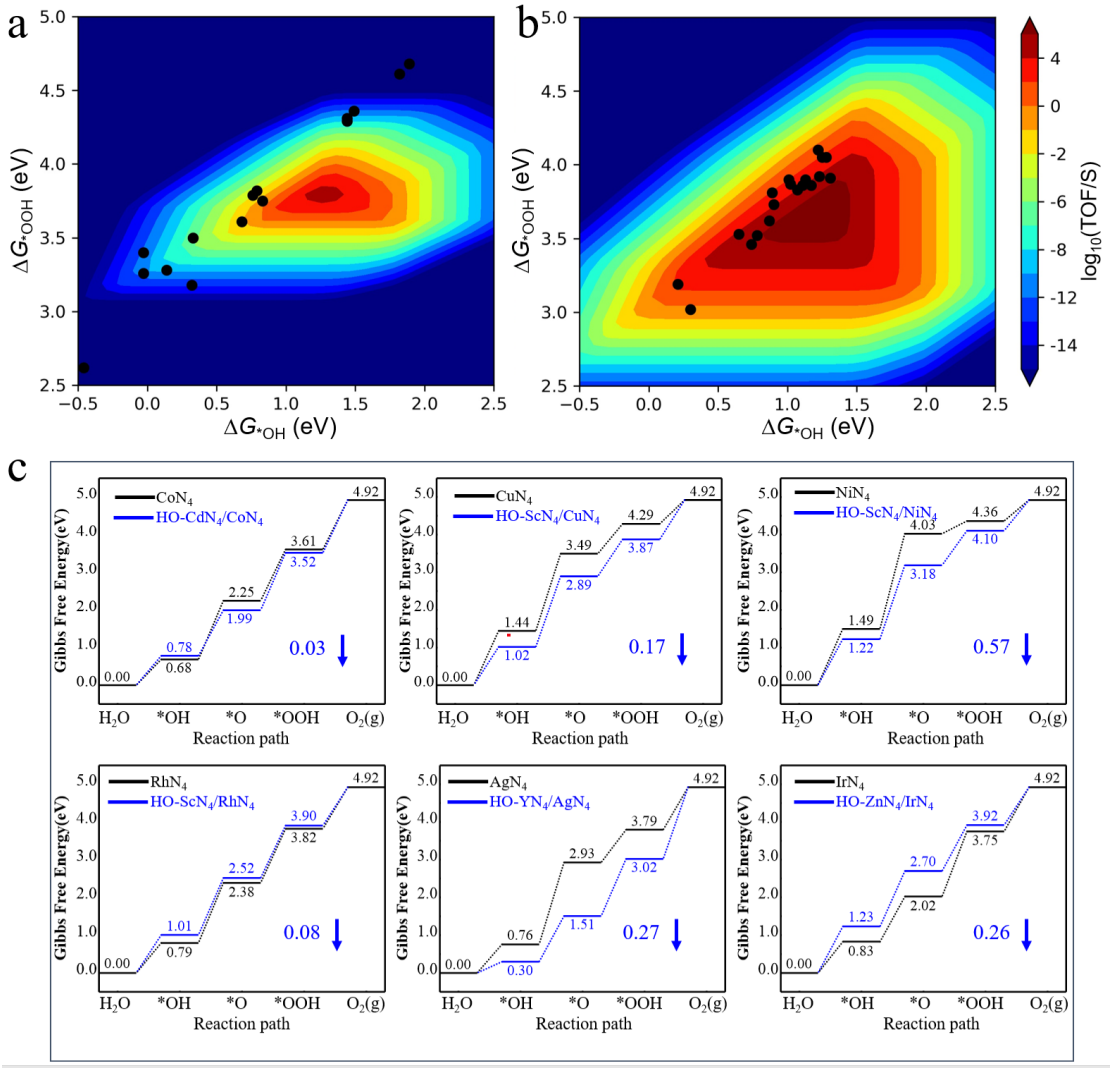

Figure 4. Oxygen evolution catalytic activity volcano maps on different active sites. Calculated OER rates as a function of the *OH adsorption energy and *OOH energy on (a) MN_4/G sites; b) $M1N_4$-$M2N_4$/G sites; c) Gibbs free energy diagrams of CoN_4/G, CuN_4/G, NiN_4/G, RhN_4/G, AgN_4/G and IrN_4/G and the respective corresponding $M1N_4$-$M2N_4$/G for OER.

Finally, we investigated how SCE of *OH(M1) alters the whole energetics of all elementary steps of OER on $M2N_4$. Overall, the presence of *OH(M1) next to M2 tends to equalize the free energy change of consecutive steps in OER (Fig. 4c). For the step of *O formation, the much weaker scaling relation between *OH and *O (Fig. 3b) due to *OH(M1) may help lower the originally large free energy changes. For CuN_4, IrN_4, and NiN_4, the analysis (Fig. 5a) of the integrated crystal orbital Hamilton population (ICOHP, a more negative value indicates stronger bonding) between M2 and O atom in *OH(M2) showed that the SCE of *OH(M1) substantially affect the bonding strength

between M2 and O atom in *OH(M2). Taking CuN_4 as an example, the ICOHP between O and Cu atom is -1.17 for *OH on single CuN_4, and increased to -1.78 in the presence of another *OH on the adjacent ScN_4 site. For the step of *OOH formation, *OH(M1) can selectively stabilize *OOH(M2) by forming either bridge-on adsorption of OOH with both M1 and M2 or hydrogen bonds between *OH(M1) and *OOH(M2) (Fig. 5b). Either way, *OH(M1) helps alter the scaling relation between *OH and *OOH by lowering the intercept, which favors the thermodynamics of OER. This geometry-based SCE for *OH(M1) is reminiscent of the promotion role of secondary ligands in enzymatic and homogeneous catalysts. Therefore, by carefully considering the local environment around active centers in high-density SACs, we can leverage the SCE to modulate their catalytic activities.

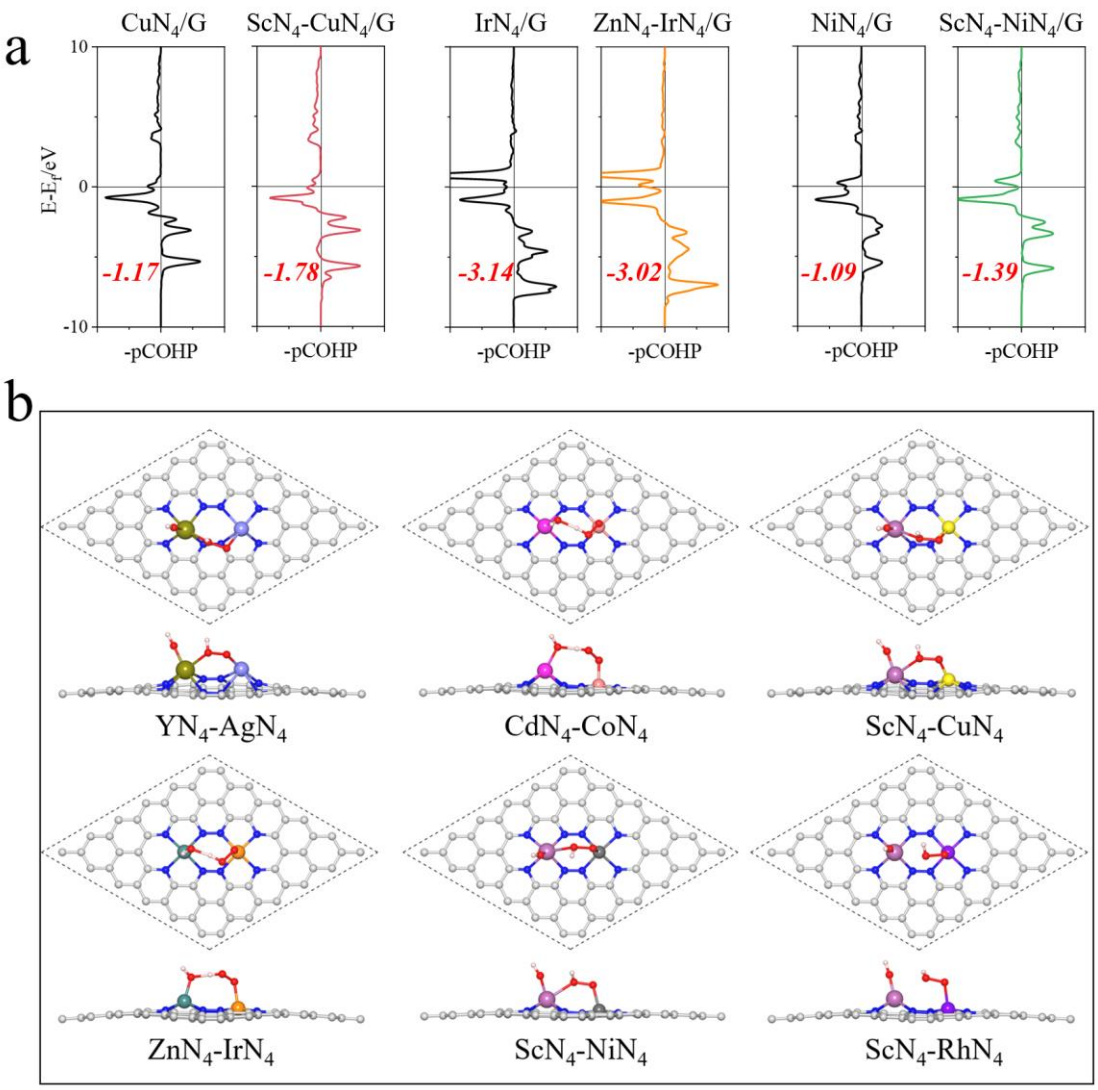

Figure 5. a) Projected crystal orbital Hamilton population (pCOHP) between the metal centers and the oxygen atom in *OH intermediate. The values of integrated COHP (ICOHP) are shown in red bold italics; b) Adsorption configurations of *OOH on M2 in $M1N_4$-$M2N_4$/G models.

Conclusion

In conclusion, our work demonstrated the existence of secondary coordination effects in high-density MN_4/G model catalysts and their impact on the scaling relationships of intermediates of OER and ORR that shape the upper limit of OER and ORR activities on these materials. By introducing the concept of secondary ligands in molecular catalysts into SACs, we successfully disrupted the linear scaling among *OH, *O and *OOH and obtained improved energetics for both OER and ORR. The kinetic simulation results supported the effectiveness of this strategy, which pushes the

calculated catalytic performance closer to the theoretical upper bound. Furthermore, the free energy diagrams indicated a remarkable reduction in the overpotential of the OER and the ORR. Our findings about SCE in high-density SACs offer valuable insight into the working mechanisms of these emerging materials and will help the rational design of SACs with enhanced performance in oxygen electrocatalysis[51].

Associated content

Supporting Information The Supporting Information is available free of charge and contains computational details, geometrical structures, and stability validation of MN_4, the adsorption energies of *OH, *O, and *OOH, various scaling relationships, and Gibbs free energy diagrams for the ORR occurring on selected $M1N_4$-$M2N_4$/G models.

Author information

Corresponding Authors

Guozhen Zhang-Hefei National Research Center for Physical Sciences at the Microscale, School of Chemistry and Materials Science, University of Science and Technology of China, Hefei, Anhui 230026, China. Email: guozhen@ustc.edu.cn

Mårten S. G. Ahlquist-Department of Theoretical Chemistry and Biology, KTH Royal Institute of Technology, 10691Stockholm, Sweden; Email: ahlqui@kth.se

Min Hu- Hefei National Research Center for Physical Sciences at the Microscale, School of Chemistry and Materials Science, University of Science and Technology of China, Hefei 230026, China. Present address: Department of Chemical and Biological Engineering, Hong Kong University of Science and Technology of China, Hong Kong. Email: humin@mail.ustc.edu.cn

Author Contributions

Ke Ye and Yulan Han contributed equally to this work.

Acknowledgments

This work is supported by the NSFC (22273093) and NKRDPC (2021YFA1500700). K.Y. and M.H.

are grateful to the support from Prof. Jun Jiang. Y.H. acknowledges the financial support from the Queen's University Belfast, the China Scholarship Council and the European Union's Horizon 2020 research and innovation program under the Marie Skłodowska-Curie Grant (agreement no. 823745). The authors are grateful for computational resources from both China and UK, including Supercomputing Center of University of Science and Technology of China, the UK national high-performance computing service, ARCHER, for which access was obtained via the UKCP consortium and funded by EPSRC grant ref EP/P022561/1, the UK Materials and Molecular Modelling Hub for computational resources, which is partially funded by EPSRC (EP/P020194/1), and the Queen's University Belfast Kelvin HPC service, which is partially funded by ESPRC (EP/T022175/1).

References

[1] Qiao, B.; Wang, A.; Yang, X.; Allard, L. F.; Jiang, Z.; Cui, Y.; Liu, J.; Li, J.; Zhang, T. Single-Atom Catalysis of CO Oxidation Using Pt_1/FeO_x. *Nat. Chem.* **2011**, *3*, 634-641.

[2] Li, Z.; Li, B.; Yu, C. Atomic Aerogel Materials (or Single-Atom Aerogels): An Interesting New Paradigm in Materials Science and Catalysis Science. *Adv. Mater.* **2023**, *35*, e2211221.

[3] Zhang, W.; Fu, Q.; Luo, Q.; Sheng, L.; Yang, J. Understanding Single-Atom Catalysis in View of Theory. *JACS Au* **2021**, *1*, 2130-2145.

[4] Li, J.; Stephanopoulos, M. F.; Xia, Y. Introduction: Heterogeneous Single-Atom Catalysis. *Chem. Rev.* **2020**, *120*, 11699-11702.

[5] Chen, F.; Jiang, X.; Zhang, L.; Lang, R.; Qiao, B. Single-Atom Catalysis: Bridging the Homo- and Heterogeneous Catalysis. *Chinese J.Catal.* **2018**, *39*, 893-898.

[6] Wang, A.; Li, J.; Zhang, T. Heterogeneous Single-Atom Catalysis. *Nat. Rev. Chem.* **2018**, *2*, 65-81.

[7] Li, L.; Chang, X.; Lin, X.; Zhao, Z.-J.; Gong, J. Theoretical Insights into Single-Atom Catalysts. *Chem. Soc. Rev.* **2020**, *49*, 8156-8178.

[8] Wang, Y.; Su, H.; He, Y.; Li, L.; Zhu, S.; Shen, H.; Xie, P.; Fu, X.; Zhou, G.; Feng, C.; Zhao, D.; Xiao, F.; Zhu, X.; Zeng, Y.; Shao, M.; Chen, S.; Wu, G.; Zeng, J.; Wang, C. Advanced Electrocatalysts with Single-Metal-Atom Active Sites. *Chem. Rev.* **2020**, *120*, 12217-12314.

[9] Zhuo, H.-Y.; Zhang, X.; Liang, J.-X.; Yu, Q.; Xiao, H.; Li, J. Theoretical Understandings of Graphene-Based Metal Single-Atom Catalysts: Stability and Catalytic Performance. *Chem. Rev.* **2020**, *120*, 12315-12341.

[10] Hannagan, R. T.; Giannakakis, G.; Flytzani-Stephanopoulos, M.; Sykes, E. C. H. Single-Atom Alloy Catalysis. *Chem. Rev.* **2020**, *120*, 12044-12088.

[11] Singh, B.; Gawande, M. B.; Kute, A. D.; Varma, R. S.; Fornasiero, P.; McNeice, P.; Jagadeesh, R. V.; Beller, M.; Zbořil, R. Single-Atom (Iron-Based) Catalysts: Synthesis and Applications. *Chem. Rev.* **2021**, *121*, 13620-13697.

[12] Kraushofer, F.; Parkinson, G. S. Single-Atom Catalysis: Insights from Model Systems. *Chem. Rev.* **2022**, *122*, 14911-14939.

[13] Xu, H.; Cheng, D.; Cao, D.; Zeng, X. C. A Universal Principle for a Rational Design of Single-Atom Electrocatalysts. *Nat. Catal.* **2018**, *1*, 339-348.

[14] Ju, W.; Bagger, A.; Hao, G. P.; Varela, A. S.; Sinev, I.; Bon, V.; Roldan Cuenya, B.; Kaskel, S.; Rossmeisl, J.; Strasser, P. Understanding Activity and Selectivity of Metal-Nitrogen-Doped Carbon Catalysts for Electrochemical Reduction of CO_2. *Nat. Commun.* **2017**, *8*, 944.

[15] Cao, L.; Liu, W.; Luo, Q.; Yin, R.; Wang, B.; Weissenrieder, J.; Soldemo, M.; Yan, H.; Lin, Y.; Sun, Z.; Ma, C.; Zhang, W.; Chen, S.; Wang, H.; Guan, Q.; Yao, T.; Wei, S.; Yang, J.; Lu, J. Atomically Dispersed Iron Hydroxide Anchored on Pt for Preferential Oxidation of CO in H_2. *Nature* **2019**, *565*, 631-635.

[16] Chen, Y.; Li, H.; Zhao, W.; Zhang, W.; Li, J.; Li, W.; Zheng, X.; Yan, W.; Zhang, W.; Zhu, J.; Si, R.; Zeng, J. Optimizing Reaction Paths for Methanol Synthesis from CO_2 Hydrogenation Via Metal-Ligand Cooperativity. *Nat. Commun.* **2019**, *10*, 1885.

[17] Zhao, W.; Zhang, L.; Luo, Q.; Hu, Z.; Zhang, W.; Smith, S.; Yang, J. Single $Mo_1(Cr_1)$ Atom on Nitrogen-Doped Graphene Enables Highly Selective Electroreduction of Nitrogen into Ammonia. *ACS Catal.* **2019**, *9*, 3419-3425.

[18] Liu, K.; Zhao, X.; Ren, G.; Yang, T.; Ren, Y.; Lee, A. F.; Su, Y.; Pan, X.; Zhang, J.; Chen, Z.; Yang, J.; Liu, X.; Zhou, T.; Xi, W.; Luo, J.; Zeng, C.; Matsumoto, H.; Liu, W.; Jiang, Q.; Wilson, K.; Wang, A.; Qiao, B.; Li, W.; Zhang, T. Strong Metal-Support Interaction Promoted Scalable Production of Thermally Stable Single-Atom Catalysts. *Nat. Commun.* **2020**, *11*, 1263.

[19] Kaiser, S. K.; Chen, Z.; Faust Akl, D.; Mitchell, S.; Pérez-Ramírez, J. Single-Atom Catalysts across the Periodic Table. *Chem. Rev.* **2020**, *120*, 11703-11809.

[20] Liu, H.; Zou, H.; Wang, D.; Wang, C.; Li, F.; Dai, H.; Song, T.; Wang, M.; Ji, Y.; Duan, L. Second Sphere Effects Promote Formic Acid Dehydrogenation by a Single-Atom Gold Catalyst Supported on Amino-Substituted Graphdiyne. *Angew. Chem. Int. Ed.* **2023**, *62*, e202216739.

[21] Stripp, S. T.; Duffus, B. R.; Fourmond, V.; Léger, C.; Leimkühler, S.; Hirota, S.; Hu, Y.; Jasniewski, A.; Ogata, H.; Ribbe, M. W. Second and Outer Coordination Sphere Effects in Nitrogenase, Hydrogenase, Formate Dehydrogenase, and CO Dehydrogenase. *Chem. Rev.* **2022**, *122*, 11900-11973.

[22] Van Stappen, C.; Dai, H.; Jose, A.; Tian, S.; Solomon, E. I.; Lu, Y. Primary and Secondary Coordination Sphere Effects on the Structure and Function of S-Nitrosylating Azurin. *J. Am. Chem. Soc.* **2023**, *145*, 20610-20623.

[23] Trouvé, J.; Gramage-Doria, R. Beyond Hydrogen Bonding: Recent Trends of Outer Sphere Interactions in Transition Metal Catalysis. *Chem. Soc. Rev.* **2021**, *50*, 3565-3584.

[24] Drover, M. W. A Guide to Secondary Coordination Sphere Editing. *Chem. Soc. Rev.* **2022**, *51*, 1861-1880.

[25] Bullock, R. M.; Dey, A. Introduction: Catalysis Beyond the First Coordination Sphere. *Chem. Rev.* **2022**, *122*, 11897-11899.

[26] Wagner, A.; Sahm, C. D.; Reisner, E. Towards Molecular Understanding of Local Chemical Environment Effects in Electro- and Photocatalytic CO_2 Reduction. *Nat. Catal.* **2020**, *3*, 775-786.

[27] Berggren, G.; Adamska, A.; Lambertz, C.; Simmons, T. R.; Esselborn, J.; Atta, M.; Gambarelli, S.; Mouesca, J. M.; Reijerse, E.; Lubitz, W.; Happe, T.; Artero, V.; Fontecave, M. Biomimetic

Assembly and Activation of [FeFe]-Hydrogenases. *Nature* **2013**, *499*, 66-69.

[28] Craig, M. J.; Coulter, G.; Dolan, E.; Soriano-Lopez, J.; Mates-Torres, E.; Schmitt, W.; Garcia-Melchor, M. Universal Scaling Relations for the Rational Design of Molecular Water Oxidation Catalysts with near-Zero Overpotential. *Nat. Commun.* **2019**, *10*, 4993.

[29] Baran, J. D.; Gronbeck, H.; Hellman, A. Analysis of Porphyrines as Catalysts for Electrochemical Reduction of O_2 and Oxidation of H_2O. *J. Am. Chem. Soc.* **2014**, *136*, 1320-6.

[30] Ye, K.; Hu, M.; Li, Q.-K.; Luo, Y.; Jiang, J.; Zhang, G. Cooperative Single-Atom Active Centers for Attenuating the Linear Scaling Effect in the Nitrogen Reduction Reaction. *J. Phys. Chem. Lett.* **2021**, *12*, 5233-5240.

[31] Ouyang, Y.; Shi, L.; Bai, X.; Li, Q.; Wang, J. Breaking Scaling Relations for Efficient CO_2 Electrochemical Reduction through Dual-Atom Catalysts. *Chem. Sci.* **2020**, *11*, 1807-1813.

[32] Busch, M.; Halck, N. B.; Kramm, U. I.; Siahrostami, S.; Krtil, P.; Rossmeisl, J. Beyond the Top of the Volcano? – a Unified Approach to Electrocatalytic Oxygen Reduction and Oxygen Evolution. *Nano Energy* **2016**, *29*, 126-135.

[33] Wang, P.; Chang, F.; Gao, W.; Guo, J.; Wu, G.; He, T.; Chen, P. Breaking Scaling Relations to Achieve Low-Temperature Ammonia Synthesis through Lih-Mediated Nitrogen Transfer and Hydrogenation. *Nat. Chem.* **2017**, *9*, 64-70.

[34] Zhao, Z.-J.; Liu, S.; Zha, S.; Cheng, D.; Studt, F.; Henkelman, G.; Gong, J. Theory-Guided Design of Catalytic Materials Using Scaling Relationships and Reactivity Descriptors. *Nat. Rev. Mater.* **2019**, *4*, 792-804.

[35] Li, X.; Duan, S.; Sharman, E.; Zhao, Y.; Yang, L.; Zhuo, Z.; Cui, P.; Jiang, J.; Luo, Y. Exceeding the Volcano Relationship in Oxygen Reduction/Evolution Reactions Using Single-Atom-Based Catalysts with Dual-Active-Sites. *J. Mater. Chem. A* **2020**, *8*, 10193-10198.

[36] Kulkarni, A.; Siahrostami, S.; Patel, A.; Norskov, J. K. Understanding Catalytic Activity Trends in the Oxygen Reduction Reaction. *Chem. Rev.* **2018**, *118*, 2302-2312.

[37] Ye, K.; Hu, M.; Li, Q. K.; Han, Y.; Luo, Y.; Jiang, J.; Zhang, G. Cooperative Nitrogen Activation and Ammonia Synthesis on Densely Monodispersed Mo-N-C Sites. *J. Phys. Chem. Lett.* **2020**, *11*, 3962-3968.

[38] Fundamental Concepts in Heterogeneous Catalysis-Wiley (2014).

[39] Zhan, S.; Ahlquist, M. S. G. Dynamics and Reactions of Molecular Ru Catalysts at Carbon Nanotube–Water Interfaces. *J. Am. Chem. Soc.* **2018**, *140*, 7498-7503.

[40] Zhan, S.; Zou, R.; Ahlquist, M. S. G. Dynamics with Explicit Solvation Reveals Formation of the Prereactive Dimer as Sole Determining Factor for the Efficiency of Ru(bda)L_2 Catalysts. *ACS Catal.* **2018**, *8*, 8642-8648.

[41] Matheu, R.; Ertem, M. Z.; Benet-Buchholz, J.; Coronado, E.; Batista, V. S.; Sala, X.; Llobet, A. Intramolecular Proton Transfer Boosts Water Oxidation Catalyzed by a Ru Complex. *J. Am. Chem. Soc.* **2015**, *137*, 10786-95.

[42] Baran, J. D.; Grönbeck, H.; Hellman, A. Analysis of Porphyrines as Catalysts for Electrochemical Reduction of O_2 and Oxidation of H_2O. *J. Am. Chem. Soc.* **2014**, *136*, 1320-1326.

[43] Liu, S.; Li, Z.; Wang, C.; Tao, W.; Huang, M.; Zuo, M.; Yang, Y.; Yang, K.; Zhang, L.; Chen, S.; Xu, P.; Chen, Q. Turning Main-Group Element Magnesium into a Highly Active Electrocatalyst for Oxygen Reduction Reaction. *Nat. Commun.* **2020**, *11*, 938.

[44] Xiong, Y.; Sun, W.; Xin, P.; Chen, W.; Zheng, X.; Yan, W.; Zheng, L.; Dong, J.; Zhang, J.; Wang,

D.; Li, Y. Gram-Scale Synthesis of High-Loading Single-Atomic-Site Fe Catalysts for Effective Epoxidation of Styrene. *Adv. Mater.* **2020**, *32*, e2000896.

[45] Shi, Q.; Zhu, C.; Du, D.; Lin, Y. Robust Noble Metal-Based Electrocatalysts for Oxygen Evolution Reaction. *Chem. Soc. Rev.* **2019**, *48*, 3181-3192.

[46] Ha, M.; Kim, D. Y.; Umer, M.; Gladkikh, V.; Myung, C. W.; Kim, K. S. Tuning Metal Single Atoms Embedded in Nxcy Moieties toward High-Performance Electrocatalysis. *Energy Environ. Sci.* **2021**, *14*, 3455-3468.

[47] Xu, H.; Cheng, D.; Cao, D.; Zeng, X. C. A Universal Principle for a Rational Design of Single-Atom Electrocatalysts. *Nat. Catal.* **2018**, *1*, 339-348.

[48] Guo, X.; Gu, J.; Lin, S.; Zhang, S.; Chen, Z.; Huang, S. Tackling the Activity and Selectivity Challenges of Electrocatalysts toward the Nitrogen Reduction Reaction Via Atomically Dispersed Biatom Catalysts. *J. Am. Chem. Soc.* **2020**, *142*, 5709-5721.

[49] Wang, P.; Chang, F.; Gao, W.; Guo, J.; Wu, G.; He, T.; Chen, P. Breaking Scaling Relations to Achieve Low-Temperature Ammonia Synthesis through Lih-Mediated Nitrogen Transfer and Hydrogenation. *Nat. Chem.* **2017**, *9*, 64-70.

[50] Medford, A. J.; Shi, C.; Hoffmann, M. J.; Lausche, A. C.; Fitzgibbon, S. R.; Bligaard, T.; Nørskov, J. K. Catmap: A Software Package for Descriptor-Based Microkinetic Mapping of Catalytic Trends. *Catal. Lett.* **2015**, *145*, 794-807.

[51] Huang, Z-F.; Song, J.; Dou, S.; Li, X.; Wang, J.; Wang, X. Strategies to Break the Scaling Relation toward Enhanced Oxygen Electrocatalysis. *Matter*. **2019**, *1*, 1494-1518.